

J. OSIKA*, H. PALKOWSKI**, K. ŚWIĄTKOWSKI*, D. POCIECHA*, A. KULA*

ANALYSIS OF MATERIAL DEFORMATION DURING THE NEW COLD TUBE ROLLING PROCESS REALIZED ON THE NEW GENERATION OF PILGER MILLS

BADANIA ODKSZTAŁCEN W NOWYM PROCESIE WALCOWANIA RUR NA ZIMNO W WALCARKACH PIELGRZYMOWYCH NOWEJ GENERACJI

The wear of tools in tube cold pilger process should be taken into consideration during process design. The working life will be longer as well as the regeneration of tool easier when the wear of tool is uniform. To obtain the uniform wear distribution the unit pressures along the working zone should be also uniform. The method of measuring of deformation distributions along the working zone were used to obtain the distribution of unit pressure.

In the paper the methods of measuring of the deformation distribution along the working zone were presented. FEM and FDM methods were used for calculations of the deformation distribution along the working zone. The direct measuring of markers displacement was presented, using the stereophotogrammetric method.

Keywords: cold pilger tube rolling, deformation measurement, finite element method, finite difference method, stereophotogrammetric method

Podczas projektowania narzędzi wykorzystywanych w procesie walcowania pielgrzymowego rur, należy uwzględnić ich zużycie. Równomierne zużycie narzędzi przedłuża ich żywotność, jak również ułatwia późniejszą regenerację. W tym celu powinno zapewnić się równomierny rozkład nacisków jednostkowych występujących w kotlinie walcowniczej. Ze względu na charakter procesu, bezpośredni pomiar nacisków jednostkowych jest niemożliwy, dlatego można wykorzystać dane dotyczące odkształceń walcowanej rury.

W niniejszej pracy zaprezentowano sposoby wyznaczania odkształceń występujących w materiale podczas walcowania pielgrzymowego. Proponowane sposoby [6], opierają się o Metodę Różnic Skończonych oraz o Metodę Elementów Skończonych. Zaprezentowano również sposób bezpośredniego wyznaczania przemieszczeń z pomiaru współrzędnych punktów przed i po wykonaniu odkształcenia. W tym celu wykorzystano metodę stereofotogrametryczną, umożliwiającą uzyskanie przestrzennego rozkładu punktów na badanej powierzchni.

Introduction

Cold rolling on the pilger mills is considered as one of the most effective manufacturing process in the case of tube production. In industry this technology is applied to the ferrous as well as non-ferrous materials even when they are hardly deformable. Mill feedstock can be deformed even up to 95% in a single operation what significantly reduces the number of required manufacturing operations and eventually lead to reduction in manufacturing costs. At the same time a high quality of the outer and inner surfaces of tubes and very high physical and mechanical material properties are obtained. A long lasting research regarding this process (called here after "conventional process") pointed out limited possibilities

of further improvements. That is why a lot of research is put on development of new generation of pilger mills.

Detailed laboratory investigation on process parameters (stress and strain distribution, varying thickness and dimensions of the sample cross-section, loads in the drive system etc.) have to be performed before industrial application. Additional problem that have to be addressed is manufacturing of appropriate tools capable to meet the process requirements.

Advantages provided by the physical modelling can be taken into account to reduce the costs of development of this new manufacturing technology. However, physical modelling of the cold pilger rolling requires highly accurate 3D experimental setup, detailed experimental

* AGH UNIVERSITY OF SCIENCE AND TECHNOLOGY, 30-059 KRAKÓW, AL. MICKIEWICZA 30, POLAND

** CLAUSTHAL UNIVERSITY OF TECHNOLOGY, ROBERT-KOCH-STRASSE 42 D- 38678 CLAUSTHAL-ZELLERFELD, GERMANY

schedules and finally appropriate model material. Results of the displacement and strain fields obtained from the developed physical model of the new generation pilger mill are presented and discussed in the present paper. This model can be considered as a real object due to the fact that it is the only prototype rolling mill capable to realize deformation according to the new idea of pilger mills. Investigation on the stress field distribution, varying thickness and dimensions of the sample cross-section and on load parameters will be the subject of further research.

1. Idea of the new cold tube rolling process realized on the new generation of pilger mill



Fig. 1. Conventional cold tube rolling process realized on the pilger mills

In contrast to other tube manufacturing processes, the cold tube rolling realized on the pilger mills has a cyclic character. In this process [1] the rolling stand

has capability to perform endwise motion. Rolls are attached to the moving rolling stand and they rotate in opposite directions as seen in Fig.1. Rolls with circular grooves and changing radius are used in this process. The groove cross-section at the entrance plane is equal to the cross-section of the initial material while at the exit plane it is equal to the cross-section of the final product. The diameter of the groove is also precisely selected. In both critical locations of the stand (rear – entrance of the initial material and front – exit of the final product) there is no contact between rolls and the material. The material is subsequently rolled along the conical mandrel bar. The rolling cycle starts when a stand is located at the rear dead location (RDL). The initial tube is then shifted by small advance distance and at the same time rotated $60 - 90^\circ$ around its axis. As a result another part of the material (volume advance) is entering the deformation zone and is rolled while the stand is moving to the front dead location (FDL). In the FDL the material is again rotated $60 - 90^\circ$ around its axis. Ovalization of the tube occurs during the reversal movement of the stand. To increase the capacity of the process and the tube deformation during reverse rolling, sometimes the advance of material is applied in FDL.

In the new cold tube rolling process the stand is fixed and the tube is placed at the slide base that enters between the rolls. The slide base performs endwise motion while rolls are fixed and performs only rotational movement. The tube is rotated when the slide base reaches critical front or rear positions, the same as in the classical approach. In this approach the stiffness of the rolling stand is increased and forces of inertia are reduced what should result in intensification of the cold pilger rolling.

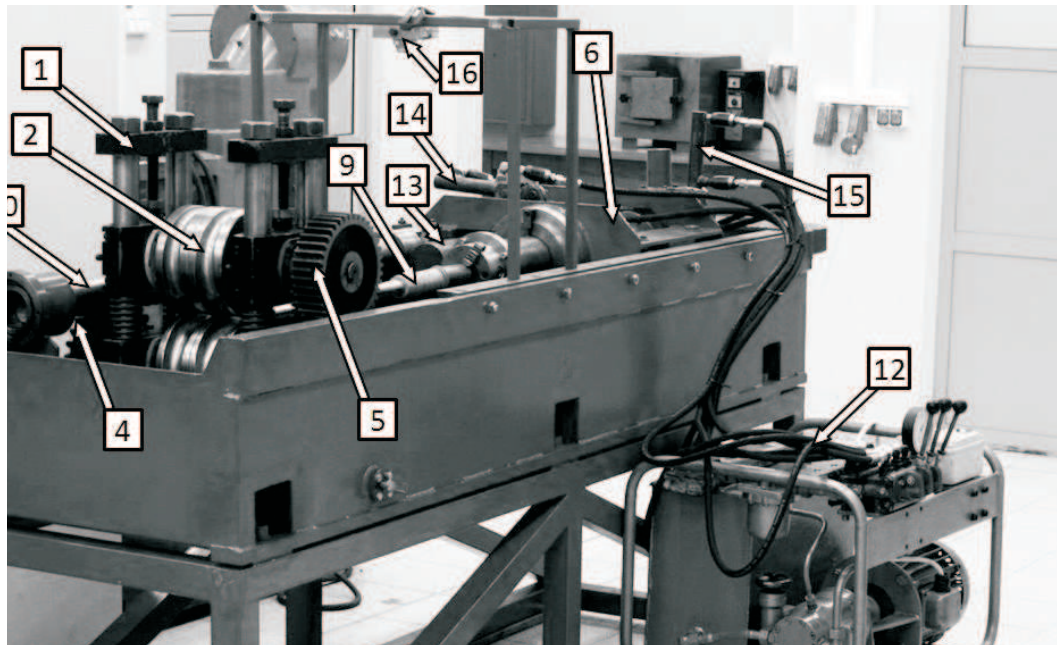
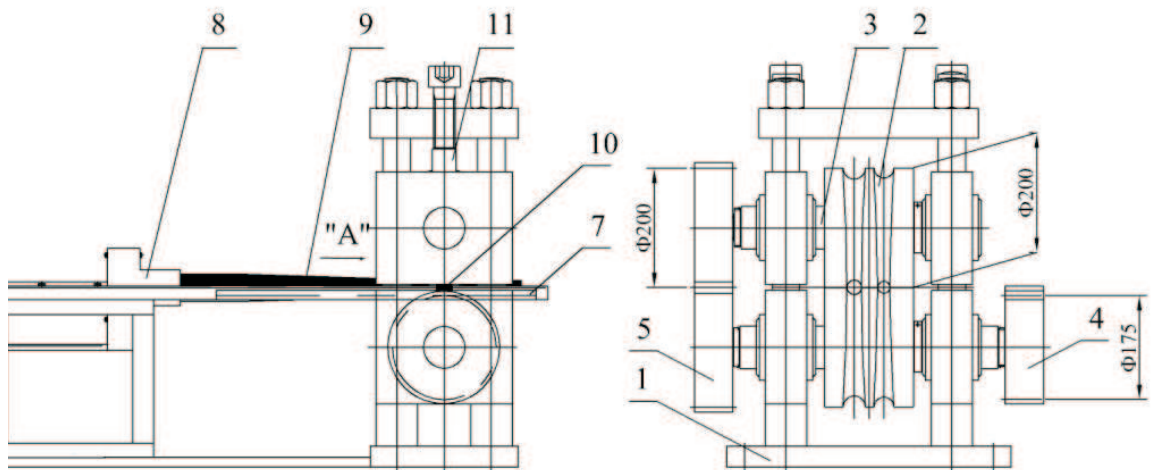


Fig. 2. The new generation of the pilger rolling mill used for the physical modelling of the tube cold rolling. (a – scheme, b – view; 1 – rolling stand, 2 – ring roll, 3 – work roll, 4 – gear wheel, 5 – transmission gear 1:1, 6 – slide base, 7 – sliding and rotating mechanism, 8 – initial tube carriage, 9 – tube, 10 – gear strip, 11 – pressure measurement system, 12 – hydraulic drive, 13 – servomotor for drive, 14 – servomotor for slide, 15 – servomotor for rotation, 16 – camera) [3]

The recent developments in the pilger rolling [2,3,4] resulted in a prototype of the new generation cold tube rolling mill. In the presented approach (Fig. 2a) the rolling stand (1) with attached rolls remains fixed during the deformation cycle. The rolls (2) rotate while the tube (9) is located at the slide base (7) performs endwise motion. Additionally, conical mandrel is placed inside the sliding base. In this concept the deformation cycle

starts when the slide base is in the FDL (exit of the final product). First the advance and 60° rotation along the tube axis take place. The deformation occurs while the slide base moves towards RDL. When the slide base stops, again the rotation of the tube occurs. The plastic deformation takes place also during the movement of the slide in FDL. In both processes a dual advance can be performed in the dead locations.

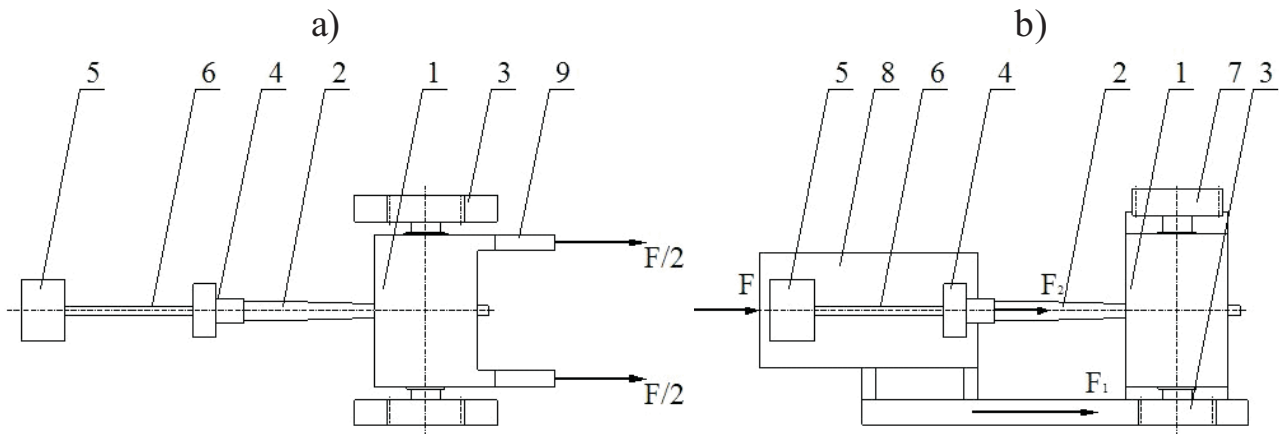


Fig. 3. Load transfer from the drive system to the rolling stand (a – conventional solution, b – solution in the new generation pilger mill; 1 – rolling stand, 2 – conical mandrel bar, 3 – gear and strip system, 4 – advance carriage, 5 – stopping pole clamp system, 6 – stopping pole, 7 – transmission gear wheel, 8 – carriage, 9 – stand connecting-rod) [2]

The approach with fixed stand significantly influences the load distribution that is transferred from the drive to the stand [3]. In the conventional approach (Fig. 3a) the loads from the connecting-rod of the stand F result in its endwise movement and in work rolls rotation. The torque is responsible for loads that result in plastic deformation of the tube in the temporary pilger roll gap. In this process there are two main loads; the vertical load F_v on rolls, and the horizontal load F_h along the tube.

In the new cold pilger rolling (Fig. 3b) the driving force from the carriage F can be divided into two components: F_1 – load in the gear strip system (results in the rolls torque) and F_2 – load along the rolled tube. In this new setup the loads are similar to the conventional approach, however, as presented in [5] the load distribution and values differ in those two approaches. As a result the stress state in the rolling gap is also different. This problem will be further investigated. The main advantages of the new cold pilger rolling process can be summarized as follows:

1. over 60% reduction in weights of the elements that perform endwise movement [3],
2. the stiffness of the fixed rolling stand can be increased without increasing the weight. There are several possibilities to increase this stiffness. Increase in the size of the stands is only one of the solution. The other solution is application of the multi roll mills. Reduction in weight of the moving parts can also result in increase in rolling velocities. Application of the hydraulic drive system can become an additional element counterbalancing inertia forces,
3. the roll diameters can increase (elongation of the deformation zone) due to the fact that rolls are fixed and perform only rotational movement,

4. optionally additional stresses can be applied along the axis and circumference,
5. possibility to use cheaper and simpler hydraulic drive,
6. preliminary cost estimation proved that modernization of the conventional pilger rolling mill according to the new idea is more than half price cheaper than the new equipment manufactured by other producers.

2. Analysis of strain distribution during the new cold pilger rolling process

2.1. The strain state evolution during pilger rolling deformation cycle

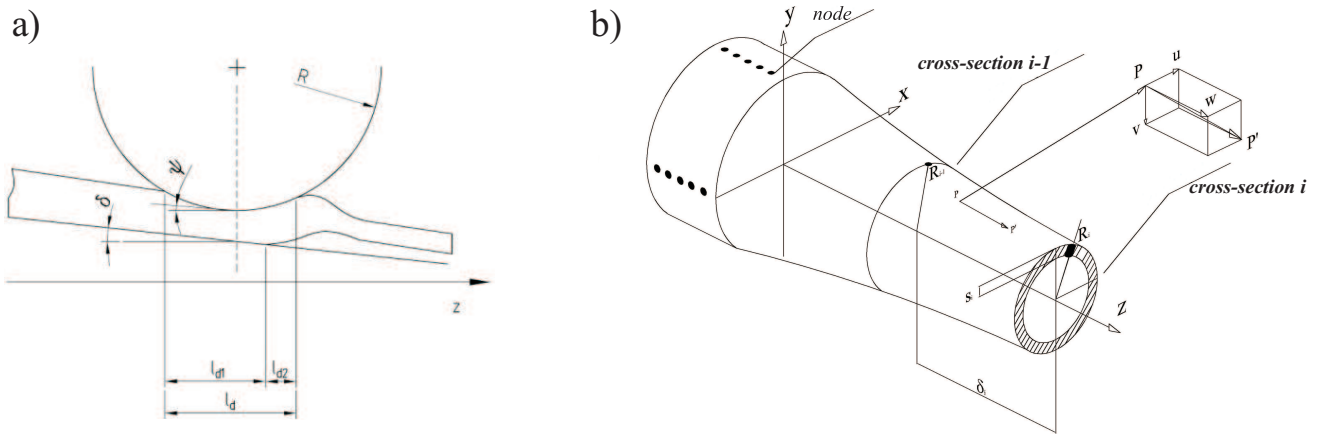


Fig. 4. a) Longitudinal cross-section of the temporary pilger roll gap, b) working cone in the Cartesian coordinate system

According to the classical theory of the pilger rolling [1], the strain state is defined both in the temporary pilger roll gap (Fig. 4a) and in the pilger rolling deformation cycle. The first is analyzed in the narrow region surrounding the present location of the working cone. The strain evolution is a result of stress state due to interactions between rolls and mandrel. The shape and dimensions of the temporary pilger roll gap are defined by the amount of deformation. Any point of the mandrel

is shifted during the single pilger rolling deformation cycle $\{u, v, w\}$ (in the x, y, z co-ordinate system):

$$\left. \begin{aligned} u &= g_1(x, y, z) \\ v &= g_2(x, y, z) \\ w &= g_3(x, y, z) \end{aligned} \right\}, \quad (1)$$

Corresponding strain components are then calculated with (2) where partial derivatives can be substituted by the difference quotient:

$$\left\| \begin{aligned} \varepsilon_x &= \frac{\partial u}{\partial x} \approx \frac{\Delta u}{\Delta x} \\ \varepsilon_y &= \frac{\partial v}{\partial y} \approx \frac{\Delta v}{\Delta y} \\ \varepsilon_z &= \frac{\partial w}{\partial z} \approx \frac{\Delta w}{\Delta z} \end{aligned} \right\| \left\| \begin{aligned} \gamma_{xy} &= \frac{\partial v}{\partial x} + \frac{\partial u}{\partial y} \approx \frac{\Delta v}{\Delta x} + \frac{\Delta u}{\Delta y} \\ \gamma_{yz} &= \frac{\partial w}{\partial y} + \frac{\partial v}{\partial z} \approx \frac{\Delta w}{\Delta y} + \frac{\Delta v}{\Delta z} \\ \gamma_{zx} &= \frac{\partial w}{\partial x} + \frac{\partial u}{\partial z} \approx \frac{\Delta w}{\Delta x} + \frac{\Delta u}{\Delta z} \end{aligned} \right\} \quad (2)$$

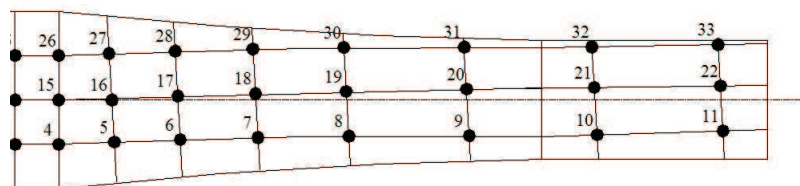


Fig. 5. Deformation grid after rolling

As a result the generating line is twisted, while the distance between nodes increases. It can be assumed that the distance in the i^{th} node with the coordinates x_i, y_i, z_i is equal to l_{i-1} and in the subsequent nodes $i + 1$ to l_i . The l_i components for the $i-1$ node with the coordinates $x_{i-1}, y_{i-1}, z_{i-1}$, can be expressed as:

$$\left. \begin{aligned} l_x^i &= \Delta x_i = x_i - x_{i-1} = \Phi_1(x, y, z) \\ l_y^i &= \Delta y_i = y_i - y_{i-1} = \Phi_2(x, y, z) \\ l_z^i &= \Delta z_i = z_i - z_{i-1} = \Phi_3(x, y, z) \end{aligned} \right\} \quad (6)$$

With the assumption that the cross section containing the i^{th} node ($i-i$) moves during the deformation by $\delta_i = m(\lambda_i - 1)$, the displacements can be calculated according to (1) as:

$$\left. \begin{aligned} u &= \Delta x_i - \Delta x_j = g_1(x, y, z) \\ v &= \Delta y_i - \Delta y_j = g_2(x, y, z) \\ w &= \Delta z_i - \Delta z_j = g_3(x, y, z) \end{aligned} \right\} \quad (7)$$

where: ($j-j$) and ($i-i$) cross sections are in the distance δi .

Similar relationships can be calculated for nodes located at the inner surface.

To solve these equations the finite difference method (FDM) with the polynomial power approach can be used. The strain state components are obtained from (2) by calculating the difference quotient. The same approach is used for calculation of the strain state at the outer and

inner surfaces of the cone die. Eventually complete 3D strain state information is obtained. However, an error in the calculations is expected due to presented earlier assumptions. That is a reason why this method can be treated as a rough estimation of the strain state during the pilger rolling. The main advantage of this approach is simplicity. The measurement of the node coordinates after rolling is the only requirement.

This method provides the possibility to calculate the strain field along the working cone in real industrial processes. However, it is very difficult to make the measurements for a single deformation cycle that last 0.4 s due to high rolling speed. However, this is not a problem in case of the laboratory pilger mill. When the slide base is in the FDL the next stroke is performed and then the first set of images is taken. This is followed by the complete deformation cycle and again a set of images is taken. The coordinates of the nodes prior and after deformation are measured on the basis of these images. Finally, the l^i components and real displacements are calculated with equations (6) and (7). These data are used to calculate the strain field during the pilger rolling. This approach is called the FDM-PO method.

Based on the authors research it can be concluded that the nodes should not be done at the beginning of the pilger rolling. First the initial material should be rolled until around 100 mm of the final tube is obtained. When the lubricant is removed from the outer and inner surfaces of the sample the nodes can be accurately put into the working cone as seen in Figure 7.

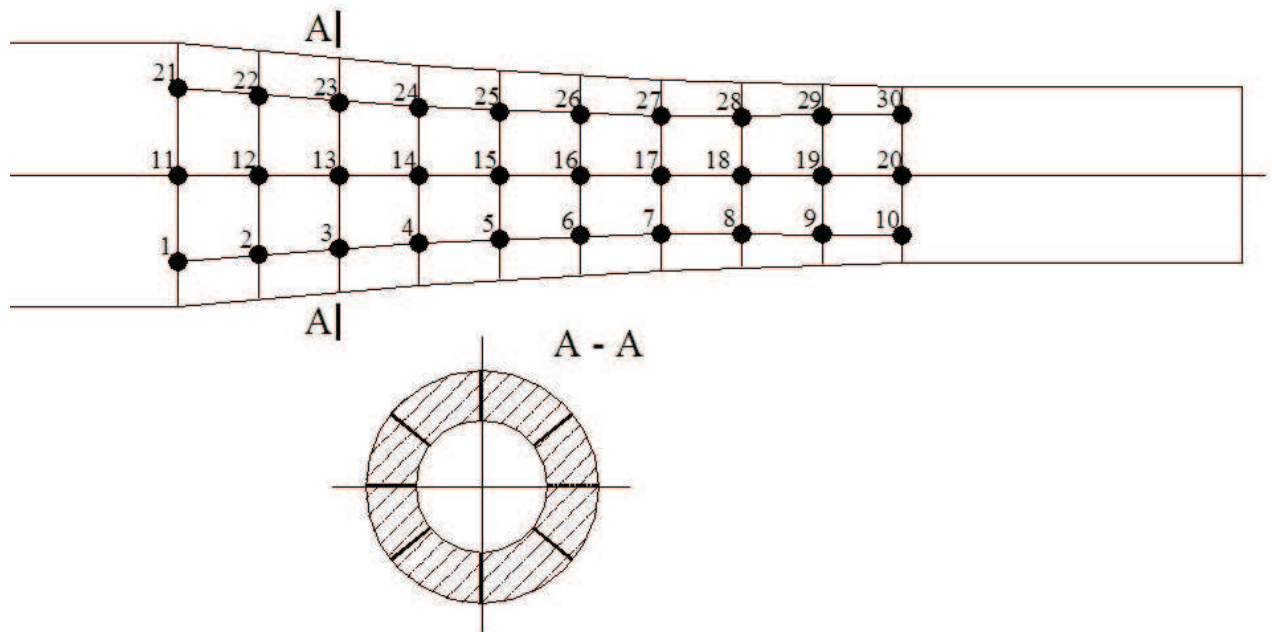


Fig. 7. Preparation stage of the working zone with nodes

The sample is attached to the slide base in the RDL and the coordinates of the nodes are measured. After the advance and rotation the carriage is moved to the RDL. While the carriage is moved backward the deformation occurs. The coordinates of the nodes are measured what is followed by rotation and advance and again the coordinates of the nodes are measured. That way displacement field can be calculated in a single cycle and separately for both directions of the carriage movement. This method is called FEM-PO. To calculate strain field a finite element method can be applied [8,9]. The interesting region is discretized with tetrahedral or hexahedral finite elements. Depending on the element type appropriate shape functions are selected and described in the matrix form:

$$\{\bar{\Delta}_i\} = \begin{Bmatrix} u \\ v \\ w \end{Bmatrix} = [N] \{\Delta_i\} = [N] \begin{Bmatrix} u_i \\ v_i \\ w_i \end{Bmatrix} \quad (8)$$

where: $\{\bar{\Delta}_i\}$ – displacement vector in the j^{th} element,
 $[N]$ – shape function matrix dependent on an element type,

$\{\Delta_i\}$ – nodal displacement vector.

The strain field can be described by:

$$\{\bar{\epsilon}\} = \begin{Bmatrix} \epsilon_x \\ \epsilon_y \\ \epsilon_z \\ \gamma_{xy} \\ \gamma_{yz} \\ \gamma_{zx} \end{Bmatrix} = [B] \{\bar{\Delta}\} \quad (9)$$

where: $[B]$ – deformation matrix.

The equivalent strain is calculated as:

$$\epsilon_i = \frac{\sqrt{2}}{3} \sqrt{(\epsilon_x - \epsilon_y)^2 + (\epsilon_y - \epsilon_z)^2 + (\epsilon_z - \epsilon_x)^2 + \frac{3}{2} (\gamma_{xy}^2 + \gamma_{yz}^2 + \gamma_{zx}^2)} \quad (10)$$

The accurate description of the strain field during the deformation cycle can be used for computer aided design of tools for the cold tube pilger rolling. Both described methods: FDM-PO and FEM-PO can also be used to describe strain field in the conventional pilger rolling.

The stereophotogrammetric approach is often used in physical modelling to measure grid nodes coordinates in the 3D space. Detailed description of this coordinates measurement method and subsequent strain field calculations can be found in [7].

2.2. Experimental measurements of the strain field during pilger rolling

Calculation of the strain field in the pilger rolling is possible after determination of the displacement field during single rolling cycle. This is done by comparison of the initial and final coordinates of nodes that are put on the sample surface prior rolling. These nodes have to be clearly visible after deformation. In the present study authors decide to use a new chemical method to put the nodes onto the surface. This method provides a grid with clearly visible nodes after deformation. High density of the nodes that at the same time are easy to distinguish from the sample surface provide very accurate measurement after deformation.

The set of orthogonal lines that eventually form a square grid is put on the sample by the silk-screen printing. The sample with the square grid is then put onto the HNO_3 acid solution to make the grid lines by etching. In the last stage the deepen grid lines are filled with tin (Sn). Example of the final grid placed on the Cu tube is shown in Figure 8.

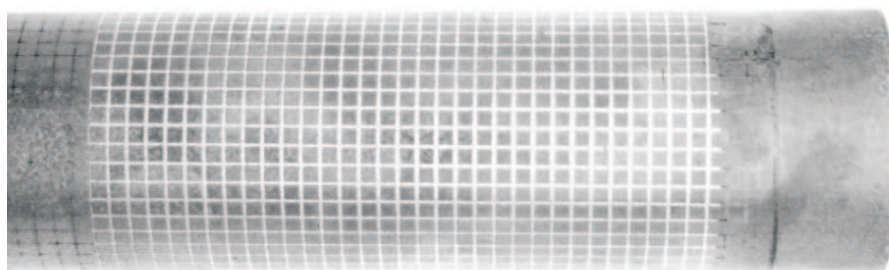


Fig. 8. Initial tube with the square grid filled with the Tin obtained by the chemical method

The initial tube with the grid is then subjected to rolling. Despite modification in this method, the grid lines are still grinded during subsequent rolling passes and eventually become close to be invisible as seen in

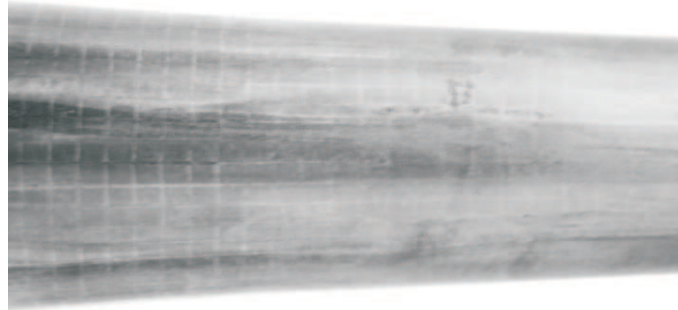


Fig. 9. Working cone with the deformed grid

To solve this problem chemical etching time of the grid can be increased in order to provide deeper grid lines for tin deposition. Another solution is to put the grid in the already prerolled sample. The sample is then rolled in one deformation cycle and location of the grid nodes can be measured.

The marker method eliminates mentioned problem with the etched grid. A series of holes is drilled in the investigated tube. These holes are then filled with the marker material. Due to the character of the tube rolling process (small diameter reduction and high elongation) the holes should be properly located. Smaller amount of holes is required along the circumference while high density of holes is required along the sample. However, the higher the density of holes along the sample is higher, the probability of influencing natural material flow

Figure 9 what makes them useless for the FotoGrant2008 recognition software. This grinding process is directly related to the high friction at the surface during the pilger rolling.

will be. The fracture initiation can also be observed in this case.

The marker material has to be selected precisely. It should have a different colour to be easily identified in the sample material. At the same time the mechanical properties and flow behaviour of both markers and sample material should be as similar as possible. If the marker material is too soft it is difficult to put it into the whole and at the same time it can be extruded from the hole during the deformation (Fig. 10b). If the material is too hard, then it will significantly affect flow of the sample material (Fig. 10c). The proper material of the markers behaves similar to the sample material and will remain in the sample during the entire rolling as seen in Figure 10d.

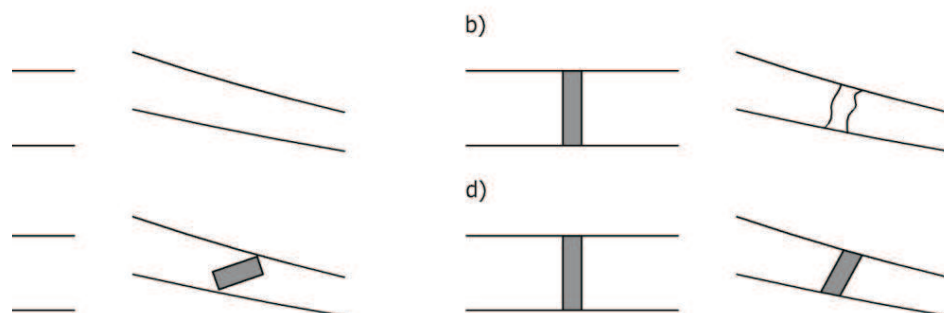


Fig. 10. The grid after n -cycles of deformation, a) grid at the surface, b) the marker material is too hard, c) the marker material is too soft, d) the marker material is properly selected

An aluminium tube (99,7% Al) with the dimension 45 x 3 mm (Fig. 11) was used during the experimental work. As grid material copper rod with diameter 1.25

mm was taken. Seven copper lines were located with 20 mm spacing along the circumference. The initial tube prior to rolling is presented in Figure 9. After n^{th} cycle

the tube is finished and is subjected to calibration process to obtain required final dimensions. After this stage a series of photos of the entire surface was taken to calculate the displacement field. Usually 30% of the surface is visible at the photograph, while only 20% can be used for calculations. After each pair of photographs is taken

the sample is rotated 30°. To cover entire tube surface usually 12 pairs of photographs were taken. After that, the last deformation cycle was performed, followed by the same procedure of taking photos to obtain all the required information for strain field calculation.

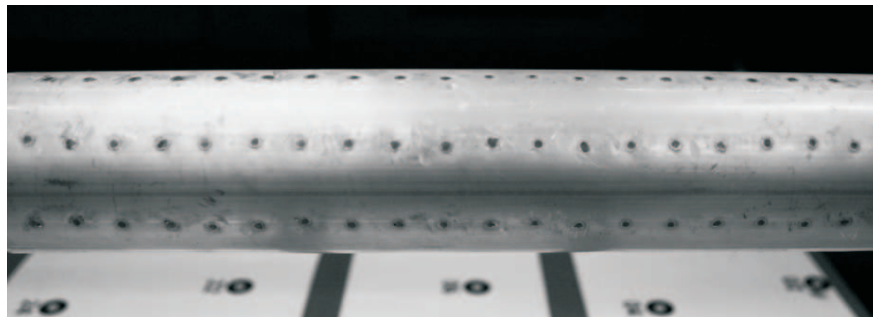


Fig. 11. Aluminium tube with markers

To obtain sharp image of the sample with markers, the photos have to be taken with the large focal depths and the long exposure time. Additional light source can be put on both sides of the tube or a flash light with the polarization can be used. However to obtain uniformly distributed light the flash light cannot be the only light

source. It is very difficult to identify the location of the grid when the sample is over-exposed or under-exposed. In that case an incorrect result will be obtained. Examples of correct and incorrect images are presented in Figure 12.

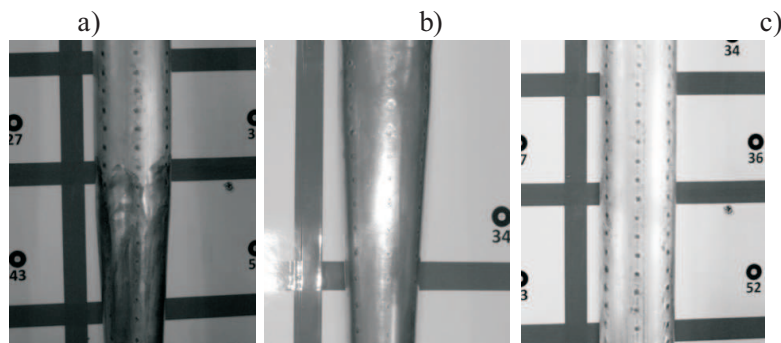


Fig. 12. The images when the scene is a) under-exposure, b) over-exposure and c) correct

The FotoGrant2008 software can process one pair of images at a time, so as results 12 different output files with the complete coordinates grid are obtained. A

series of simple geometrical transformations are applied (e.g. rotation along the rolling direction) to reconstruct the complete surface of the final tube (Fig. 13a,b).

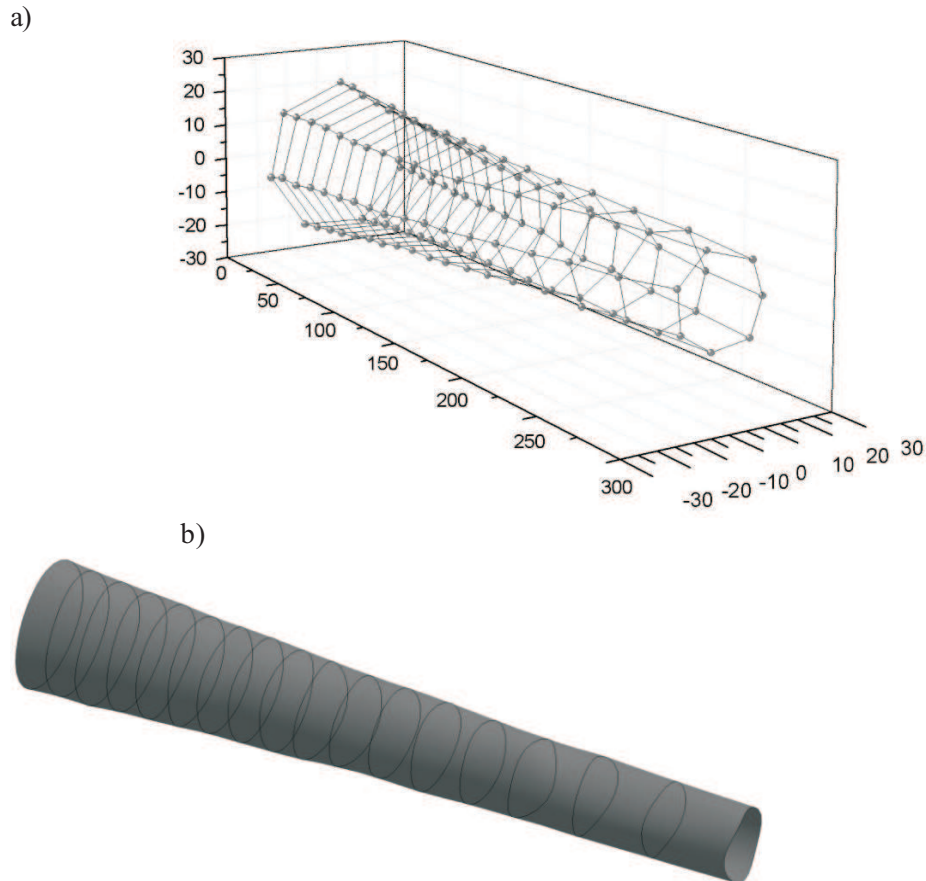


Fig. 13. a) Coordinates of the grid points from the FotoGrant2008 software, b) completed reconstruction of the tube surface

The measurement errors in this method are related to: δ_f – the measurement error in FotoGrant2008 software, δ_d – the error due to setup of the physical model, δ_p – the error due to manual overlaying of the measurement grid elements.

The δ_f is calculated as a difference between location of a measured coordinates and the base coordinates saved in the software. Each difference has to be smaller than $0.5px$. When images with the 3872×2592 resolution are considered, the error is small and can be neglected.

To minimize error related to the method setup δ_d , it is necessary to assure precise rotation angle of the camera around the tube axis as well as accurate determination of the axis position. The stereophotogrammetric method is used to determine this position with the accuracy 0.1mm and laser radar is used to assure the proper position of the tube axis. Because of it the δ_d is small and also do not influence on the total error of this method.

The total error of this method depends mostly of the value of δ_p error. The markers are deforming and they are not always in the centre of the marker surface. These small shifts (around several pixels) results in the error equal to several decimal millimetre. These errors accumulate during the measurements.

One of the main advantages of this method is the possibility to reconstruct displacement at the outer and inner tube surfaces. However, this is an example of an invasive measurement method what limits density of the grid. When the density is too high it significantly influence the character of material flow during tube rolling. This process is also very time consuming. Usually several thousand of measurement points are required to obtain accurate results. That is a reason why a lot of researches are put on automation of these measurements by using image recognition software. Automatic determination of the marker centres would significantly reduce measurement time and increase accuracy of the obtained results.

2.3. Calculation of the strain field during the pilger rolling

The 45x3 mm aluminium tube with the copper markings located in 20 mm distance along circumference and 10 mm length was used during the research. The single stroke 4 mm/cycle and the 60° rotation at the FDL were applied. The final tube dimensions are 24.7x1 mm. As presented earlier, a series of images was taken prior and after six deformation steps to calculate the $\{u, v, w\}$ displacements according to eq. (7).

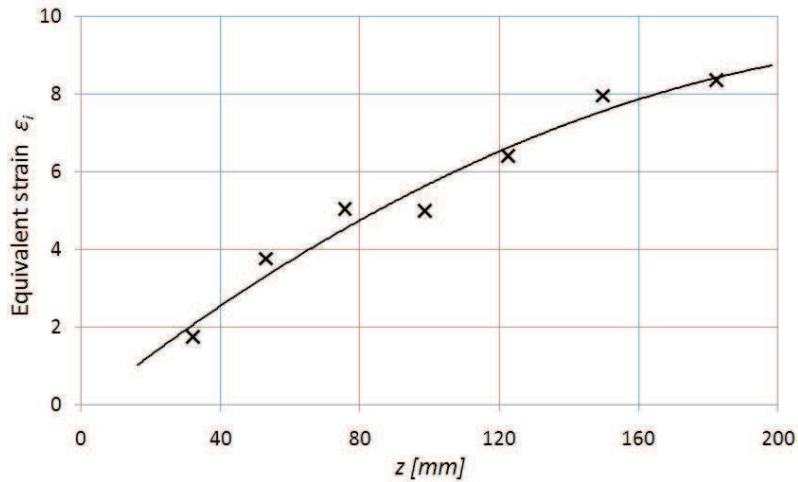


Fig. 14. The obtained equivalent strain ϵ_i along the rolling tube

The obtained equivalent strain values measured on the outer tube surface along the tube are shown in Fig. 14. Obtained displacement values $\{u, v, w\}$ are comparable to the measurement errors and this significantly affects further calculations. Eventually, the obtained results are different to the real values. As mentioned earlier, this method should be considered as rough estimation of material behaviour during deformation. Nevertheless, the obtained results have consistent character with the experimental observations: the deformation is the smallest at the entrance to the rolling gap and increases with the strain hardening.

3. Conclusions

1. The experimental determination of the 3D displacement and strain fields during the cold pilger rolling is very demanding task. In practice, due to large rolling velocities it is limited only to one deformation cycle. Eventually the method FDM-PO described in chapter 2.1, can be applied to determine locations of the marking grid after deformation. Much better results can be obtained with application of the physical modelling of the strain field distribution during pilger rolling, because coordinates of the marking grid can be measured prior and after single deformation cycle. The possibilities of this approach were confirmed within the paper.
2. One of the major problems in the proposed method is an appropriate distribution of the markings on the outer and inner tube surfaces to obtain dense evenly spaced marking grid. Because of high deformation and friction of the pilger rolling the grids are disappearing and accurate displacement measurement becomes difficult. The less accurate and invasive method of measurements nodes located in the drilled holes along the tube was used in the paper. Because the lengths of the sides were too large, the accuracy of measurements were not sufficient. The problem of node distribution at the inner surface of the tube and along the cone surfaces was not solved in the paper and remains open for further research. Verification of the FEM-PO method will also be the subject of further work.
3. The developed stereophotogrammetric approach based on the FotoGrant 3D software to determine 3D node coordinates is very useful. The obtained results pointed out possible errors as well as possibilities to solve them. To facilitate and automate the measurements complex software has to be developed. At this stage the measurements are manually loaded into the FotoGrant software what significantly decreases the accuracy and increases time required for the method.
4. The results obtained were presented in chapter 2.3. However, at this stage due to large calculation errors these results cannot be used as valuable data during the process of e.g. tool design. Additionally, obtained results are only for the outer surface of the tube. The obtained strain field cannot be considered as 3D, because the inner surface is neglected during calculations. Nevertheless, the general character of the results is in agreement with the theory and with the results obtained using other methods [1]. It can be concluded that the FDM-PO is an appropriate tool for the strain field determination.
5. The problem of measurements of the varying thickness and dimensions of the sample cross-section along the deformation gap in the pilger rolling will be the subject of further investigation.

REFERENCES

- [1] J. Osika, Walcowanie rur na zimno w walcarkach pielgrzymowych, Uczelniane Wydawnictwa Naukowo – Dydaktyczne AGH, (2004).
- [2] J. Osika, C. Boberek, A. Machnik, S. Nowak, R. Perlega, M. Repeła, S. Starzykowski, A. Pietrzak, Walcarka pielgrzymowa do wytwarzania rur na zimno – zgłoszenie wynalazku w Urzędzie Patentowym RP nr P – 375655 z mocą od dnia 09.06. 2005 r.
- [3] J. Osika, Nowa koncepcja procesu walcowania rur na zimno w walcarkach pielgrzymowych, Rudy i Metale Nieżelazne **11**, 629-634 (2006).
- [4] J. Osika, K. Świątkowski, Ł. Karaś, Modelowanie fizyczne walcowania na zimno rur w walcarkach pielgrzymowych nowej generacji, Rudy i Metale Nieżelazne **11**, 750-757 (2007).
- [5] J. Osika, K. Świątkowski, D. Pocięcha, Parametry siłowe pielgrzymowania rur na zimno w walcarkach nowej generacji, Rudy i Metale Nieżelazne **11**, 675-679 (2008).
- [6] J. Osika, K. Świątkowski, An investigations of displacement and deformation during cold rolling of tubes in pilgering process, 7th ICTP, Advanced Technology of Plasticity, Oct. 27 – Nov. 1 2002, Yokohama, Japan, v.1, 661-666 (2002).
- [7] J. Osika, D. Pocięcha, M. Piwowarska, Stereofotogrametryczna metoda wyznaczania pól przemieszczeń w walcowaniu pielgrzymowym rur na zimno – to be prepared.
- [8] M. Pietrzyk, Metody numeryczne w przeróbce plastycznej metali, Wydawnictwa AGH (1992).
- [9] O. C. Zienkiewicz, Metoda elementów skończonych, Arkady (1972).

